Chem Soc Rev

REVIEW ARTICLE

View Article Online
View Journal | View Issue

Cite this: *Chem. Soc. Rev.*, 2016, 45, 3731

Heterogeneous chemistry and reaction dynamics of the atmospheric oxidants, O_3, NO_3, and OH, on organic surfaces

Robert C. Chapleski Jr., Yafen Zhang, Diego Troya and John R. Morris*

Heterogeneous chemistry of the most important atmospheric oxidants, O_3, NO_3, and OH, plays a central role in regulating atmospheric gas concentrations, processing aerosols, and aging materials. Recent experimental and computational studies have begun to reveal the detailed reaction mechanisms and kinetics for gas-phase O_3, NO_3, and OH when they impinge on organic surfaces. Through new research approaches that merge the fields of traditional surface science with atmospheric chemistry, researchers are developing an understanding for how surface structure and functionality affect interfacial chemistry with this class of highly oxidizing pollutants. Together with future research initiatives, these studies will provide a more complete description of atmospheric chemistry and help others more accurately predict the properties of aerosols, the environmental impact of interfacial oxidation, and the concentrations of tropospheric gases.

Received 8th May 2015

DOI: 10.1039/c5cs00375j

www.rsc.org/chemsocrev

I. Introduction

O_3, OH, and NO_3 are the most important atmospheric oxidants due to their high chemical potentials, abundance, and negative effects on human health. While the importance of these oxidants has led many scientists to investigate their gas-phase chemistry,[1–4] detailed studies into the reactions of O_3, OH, and NO_3 at the gas–surface interface have only recently been reported. Interfacial reactions between organic particles and oxidative gases result in changes in particulate composition, size, and physical properties. These changes affect human health and visibility, climate, and the global carbon cycle.[5–7] Organic particles in the atmosphere form or grow through the following four mechanisms (Fig. 1): (i) biogenic emissions in remote regions and anthropogenic emissions in urban areas, which result in particles described as soot or primary organic aerosols;[8–10] (ii) adsorption of volatile organic compounds onto liquid or solid surfaces, which results in aerosols coated by organic films;[11,12] (iii) coagulation of smaller carbonaceous nanoparticles;[13] and (iv) reactions of atmospheric oxidants on the surfaces of existing organic particles, which produce so-called secondary organic aerosols (SOAs).[14,15] The concentrations of these types of organic aerosols typically range from 1 to 10 μg m^{-3} and can reach levels exceeding 15 μg m^{-3} in heavily industrialized environments.[16,17] Once formed, they nearly immediately begin contributing to the heterogeneous chemistry of the lower atmosphere.

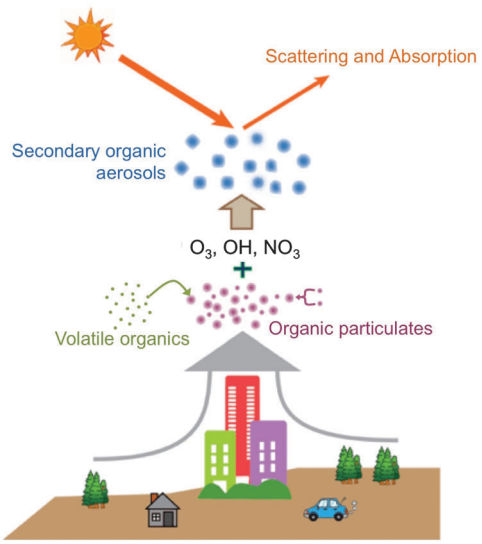

Fig. 1 Schematic illustration of the generation and transformation of organic particles in the atmosphere. Particles can form and grow from biogenic and anthropogenic emission products, adsorption of volatile organics onto surfaces, coagulation of carbonaceous nanoparticles, and reactions of atmospheric oxidants on the surfaces of existing organic particles. These particles can affect the balance of incoming and outgoing solar radiation.

Surface reactions involving O_3, NO_3, and OH are known to alter the properties and fate of organic particulates, often in unexpected ways. For example, Fig. 2 shows scanning-electron

Department of Chemistry, Virginia Tech, Blacksburg, Virginia 24061, USA. E-mail: jrmorris@vt.edu; Tel: +1-540-231-2471

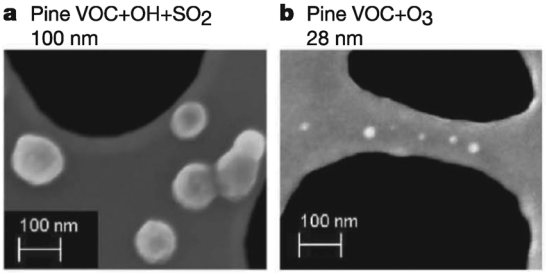

Fig. 2 SEM images of SOA particles of different sizes resulting from the oxidation of pine-seedling volatile organic compound (VOC) emissions following (a) OH-initiated oxidation in the presence of SO_2, and (b) O_3-initiated oxidation. The white spots are SOAs supported on a lacey carbon grid (black regions). Reprinted with permission from Macmillan Publishers Ltd: *Nature*, 2010, **467**, 824. Copyright 2010.

microscope images of SOAs generated through the oxidation of volatile organic emissions from pine seedlings.[18] When exposed to OH in the presence of SO_2, particles (shown as white spots in the figure) with an average radius of 100 nm are formed. Conversely, exposure to O_3 results in the formation of significantly smaller particles (28 nm). Such modifications in particulate properties due to atmospheric oxidation most likely affect the scattering and absorption of light by the particles, thereby altering the balance between incoming and outgoing solar radiation[5,19] (Fig. 1). Further, the overall surface area of each individual particle is altered, thereby affecting the subsequent adsorption and reaction rates on these surfaces. These findings have motivated scientists to investigate the role of organic surfaces in atmospheric interfacial oxidative reactions—the chemistry contributing to atmospheric organic particle transformation and growth.[20–23] Such chemistry is particularly important in polluted regions of the atmosphere where elevated concentrations of both particulates and oxidative gases often coincide.

Tropospheric O_3 has been recognized as a worldwide environmental problem, hallmarked by the presence of NO and NO_2 in the lower atmosphere. Anthropogenic O_3 first became of concern as an atmospheric pollutant in the late 1940s,[24] when high concentrations were reported in the Los Angeles area. Since then, dangerously elevated tropospheric concentrations have been measured in Greece, Japan, Sydney, Jerusalem, Mexico City, and many other locations.[19,25–27] Today, tropospheric O_3 concentrations are monitored to characterize the extent of air pollution in urban areas, where emissions from transportation and industrial plants are substantial. Anthropogenic O_3 is primarily generated from the reaction of atmospheric O_2 with ground-state $O(^3P)$ radicals that result from the photolytic dissociation of ambient NO_2[19,28] (Scheme 1).

Though air pollution is often evaluated using O_3 concentrations, hydroxyl (OH) radicals also play a critical role in daytime atmospheric chemistry. In fact, concentrations of OH radicals are difficult to quantify precisely because of their high reactivity

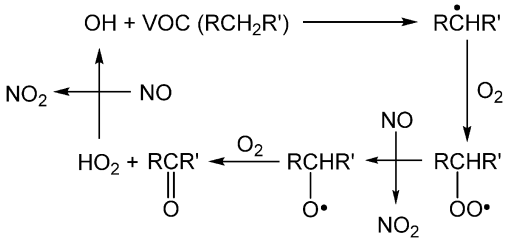

Scheme 2 Generation of NO_2 during typical oxidation of volatile organic compounds (VOC) by OH.

and consequent short atmospheric lifetime ($\leq$1 s). Techniques for quantifying OH have been reviewed by Heard and Pilling.[29] One important reaction of OH involves volatile organic compounds (VOCs) and the conversion of two molecules of NO to NO_2 (Scheme 2).[30] This conversion is primarily responsible for the formation of NO_2, a precursor to O_3 in the atmosphere (Scheme 1).[30,31] Further, the atmospheric concentration of OH is dependent on the photodissociation of O_3 by UV radiation, which produces an electronically excited oxygen atom ($O(^1D)$), able to undergo rapid reactions with water vapor in the air to form two OH radicals (Scheme 3).[32,33]

Because the primary mechanisms of O_3 and OH generation involve the photodissociation of other atmospheric molecules, reactions initiated by these two oxidants are of highest importance during the daytime.[28,32] At night, in the absence of photochemical reactions, the consumption of O_3 and OH is much faster than the formation of these two oxidants, and their atmospheric concentrations diminish.[22,34] However, oxidation of NO_2 by O_3 generates NO_3, which drives a great deal of tropospheric nighttime chemistry.[26,35] Interestingly, NO_3 chemistry is most relevant to the atmosphere after sunset because NO_3 photodissociates rapidly in daylight.[26,36] NO_3 initially reacts with certain VOCs through addition or hydrogen abstraction reactions, ultimately yielding peroxyacetyl nitrate (PAN).[37–40] PAN (due to its eventual photo- and thermal-decomposition into NO_2) acts as a reservoir and a transportation medium for NO_2.[41] In addition, reactions of NO_3 and NO_2 result in the production of dinitrogen pentoxide (N_2O_5), which is an important source of nitric acid in the atmosphere.[36]

While the rich interplay amongst O_3, OH, and NO_3 and their reactions in the gas phase have key implications in tropospheric chemistry, this review focuses on reactions of each of these gases with organic surfaces. These heterogeneous reactions alter the size and composition of atmospheric particulates and modify the surfaces of other anthropogenic and natural materials as well, such as metals, metal oxides, and polymers. The importance of these processes has provided ample motivation for detailed laboratory investigation. Below, we highlight a subset of key studies into the chemistry of organic materials with O_3, OH, and NO_3. For each gas, the review begins with a focus on

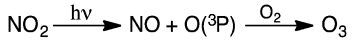

Scheme 1 Generation of O_3 in the atmosphere during the daytime.

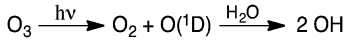

Scheme 3 Formation of OH radicals in the atmosphere during the daytime.

reactions at highly relevant, yet relatively uncharacterized, surfaces and particles (including soot), followed by studies performed with model aerosols composed of a single type of molecule or surface-adsorbate combination. Finally, each section concludes with a discussion of fundamental research involving highly ordered synthetic surfaces that helps provide insight into specific details of the gas–surface reaction dynamics and kinetics, while serving as a valuable benchmark for theoretical studies.

II. O_3 reactions with organic surfaces

Reactions between ozone and organic surfaces have long been recognized as critical to the overall chemistry of the atmosphere. It is therefore not surprising that, relative to NO_3 and OH radicals, there have been many studies into the interfacial chemistry of ozone. In the gas phase, O_3 initiates reactions with vinyl-containing organics and polycyclic aromatics *via* addition across double bonds to form an unstable primary ozonide, which triggers a series of subsequent reactions.[42–44] Analogous chemistry may occur on surfaces;[45–47] however, scientists are only beginning to decipher how surface structure and functionality affect ozone accommodation, diffusion, and reaction pathways. A quintessential result for these processes is the reactive uptake coefficient: the probability that a gas-phase molecule that collides with the surface will react with the surface. For a thorough explanation of this coefficient in terms of reactions of oxidative gases with organic surfaces, the reader is referred to work by Houle *et al.*[48]

In an investigation of the reaction kinetics of ozone with several different polycyclic aromatic hydrocarbon (PAH) compounds on laboratory-generated soot, Bedjanian and Nguyen[49] found that fast initial consumption of ozone was followed by rapid irreversible changes in the molecules at the interface, rendering the surface unreactive to further ozone exposure. In complementary work, Disselkamp and coworkers[22] investigated the reaction between soot and ozone in a static aerosol chamber. By interpreting ozone and CO_2 infrared signals over the course of ozone exposure, they obtained a stoichiometry of two O_3 molecules for every molecule of CO_2 product formed and reported a very small pseudo first-order reaction probability of 10^{-8} for ozone with "aged" soot. The interfacial reactivity of ozone on soot has also been reported in a recent study by Browne *et al.*, which yielded an uptake coefficient of 2×10^{-7}.[50] The He group further augmented these findings by performing *in situ* Raman and infrared studies[51,52] of ozone reactions with soot. Their work suggested that amorphous carbon and disordered graphitic sites were responsible for initiating the reactions. They also revealed that some of the reaction products included surface-bound ketone, lactone, and anhydride groups. Other research teams extended this work to specific surface-bound compounds (including polycyclic aromatics,[43,53–58] biogenic volatile organics,[59] biomass burning products,[60] and fungicides[61]) and functionalities at well-characterized aerosol surfaces.[62–66]

Within the body of literature on O_3 reactions with aerosols, investigations of the ozonolysis of oleic acid aerosols are of particular interest because these particulates appear in relative high abundance in certain regions of the atmosphere.[67–70] From these studies, reactive uptake coefficients have been determined to be generally on the order of 10^{-3}.[67–69,71] Variations in this coefficient have been attributed to the effects of particle size on diffusion of O_3 into the bulk[68] and the likelihood of secondary reaction pathways beyond ozonolysis.[69] Further, in an experiment in which the substrate was not uniformly covered by oleic acid, a reactive uptake coefficient on the order of 10^{-5} was found.[71] Importantly, the use of fresh surfaces in these studies contributed to a higher reactive uptake coefficient than in experiments employing passivated surfaces.[22]

Motivated by the challenge of building a highly fundamental understanding of interfacial ozone chemistry, several groups have explored ozone reactions with organic particles adsorbed onto extended (planar) solid surfaces. In their work, Ham and Wells[72] identified products formed during exposure of alpha-terpineol on glass and vinyl flooring tile to ozone. Kahan *et al.* implemented fluorescence spectroscopy in a Teflon reaction chamber to investigate the degradation kinetics of PAHs adsorbed on a microscope slide,[73] and Kwamena *et al.*[74] investigated the role of relative humidity and ozone concentration in the kinetics of ozonolysis of anthracene deposited on a pyrex flow tube. In research highlighted in these two works, the Langmuir–Hinshelwood mechanism, whereby the impinging ozone molecule thermally accommodates on the surface before reacting, adequately describes the time-resolved data.

To add insight to the role of the interaction between organic molecules and the underlying surfaces on which they are supported on oxidation reactions, Chu *et al.*[21] used density functional theory methods to model the ozonolysis of surface-bound planar PAHs. They found an energetic expense to reaction resulting from the "lift-off" of the molecules from the surface as the planar PAH reactants form nonplanar intermediates or products. Fig. 3 shows structures and energies for the ozone reaction with one of the available double bonds in pyrene. The first step in the reaction is an exoergic addition to form a primary ozonide, which retains planarity. Decomposition of the primary ozonide in step 2 leads to a non-planar Criegee intermediate. The reaction Gibbs energy (ΔG_{rxn}) for this step is +14.8 kcal mol^{-1}, and the energetic penalty resulting from loss of interactions with the underlying surface increases the reaction Gibbs energy by an additional $\sim$14 kcal mol^{-1}, with variations depending on the nature of the surface (*e.g.*, fly ash *vs.* NaCl). The last step of the reaction is the thermodynamically favorable formation of a secondary ozonide (step 3), which results in a planar species.

Additionally, attenuated total reflectance infrared (ATR-IR) experiments[75–78] have been used to investigate the effects of temperature,[75–77] relative humidity,[75–77] and film thickness[77] on reaction mechanisms,[76] product yields,[76,78] product hygroscopicity,[75,77,78] and redox activity.[75] As ATR-IR allows for *in situ* collection of infrared spectra, the change in the IR intensity of specific vibrational modes during exposure can be used to obtain kinetic information such as ozone's reactive uptake coefficient, which has been determined to be in the range of 1.0×10^{-5},[76] to 5.1×10^{-4}.[75] The measured variations in ozone

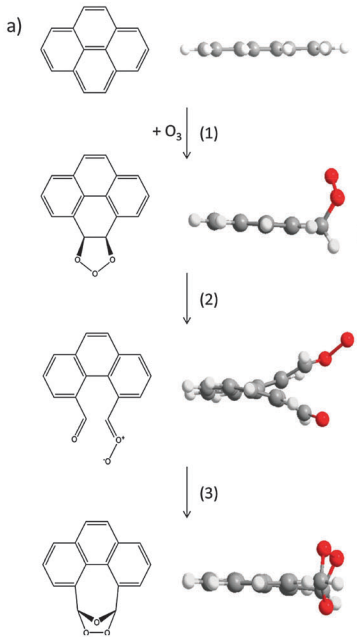

b)

reaction	ΔG_{rxn} (kcal mol^{-1}) B3LYP/6-31G**	degree of desorption, ζ	$\Delta G_{rxn} + \zeta\Delta G_{des}$ (kcal mol^{-1}) fly ash	soot	NaCl	urban aerosol
1	−23.4	0	−23.4			
2	+14.8	10/16	+31.4	+28.9	+27.0	+27.5
3	−55.2	0	−55.2			

Fig. 3 (a) Structures of minima in the oxidation of pyrene by ozone show a diversion from planarity in an intermediate. (b) Energetics of reaction steps in (a) show an energetic penalty for surface liftoff as a result of loss of planarity. ΔG_{rxn} is determined with gas-phase molecules (surface-absent), ς is defined as the fraction of carbon atoms that leave the plane of the molecule, and ΔG_{des} is the energy of complete desorption from the surface. Reprinted (adapted) with permission from *J. Am. Chem. Soc.*, 2010, **132**, 15968. Copyright 2010 American Chemical Society.

uptake coefficients are likely related to differences in the reaction conditions, surface properties, and the particular infrared band analyzed to extract kinetic information.

Beyond solid surfaces, the ozonolysis of organic compounds at the air–water interface has also been studied in thin films. Raja and Valsaraj[79] investigated the impact of ozone exposure on the rate of naphthalene vapor uptake onto single droplets of water. They reported that reactions between ozone and naphthalene at the air–water interface increased the rate of naphthalene uptake onto the droplet surface. Oxidation products with higher water solubility than naphthalene more readily diffused into the bulk, thus allowing for greater mass transfer of naphthalene from the gas phase to the surface of the droplet. Moreover, the rate of the heterogeneous ozone-naphthalene reaction—15 times greater than that of the homogeneous gas-phase reaction—was found to be dependent upon the size of the droplet. Wadia and coworkers[80] used an experimental flow chamber and molecular dynamics simulations to investigate the ozonolysis of saturated and terminally unsaturated phospholipid molecules at the air–water interface. No reaction with the saturated compound was observed, yet reaction with the unsaturated compound yielded an aldehydic product. This reaction was facilitated by the availability of the C=C double bond at the interface, which was observed to be invariant to surface film compression. Recently, Mmereki *et al.*[81] provided additional insight into the ozone-anthracene reaction in organic films on water *via* laser-induced fluorescence. Interestingly, the presence of organic acids in the aqueous phase reduced the reaction rate with the organic film, and the presence of alcohols enhanced the overall rate of reaction.

The dependence of the ozone reaction rate with organic surfaces on the physical properties of the surface has received additional scrutiny. Of particular interest, Moise and Rudich[82] noted an order-of-magnitude increase in the reactive uptake coefficient for ozone at liquid organic surfaces relative to solid samples (Fig. 4). This result was attributed to the participation of subsurface layers in liquid uptake, which is not as prevalent when the organic surface is frozen. In the figure, dashed lines mark differences in coefficients of the same compound resulting from a liquid/solid phase change. The coefficient for linoleic acid decreased from $(1.2 \pm 0.2) \times 10^{-3}$ to $(1.4 \pm 0.1) \times 10^{-4}$ upon freezing. For oleic acid, a decrease from $(8.3 \pm 0.2) \times 10^{-4}$ to $(5.2 \pm 0.1) \times 10^{-5}$ was observed. This change of phase also caused a decrease in the coefficient of 1-hexadecene from $(3.8 \pm 0.6) \times 10^{-4}$ to $(2.5 \pm 0.4) \times 10^{-5}$. These differences are similar in magnitude to those observed for liquid-phase uptake compared to a well-ordered thin film.[83] In particular, 1-octene exhibited a decrease in the uptake coefficient from 1×10^{-3} for liquid to 1×10^{-4} for a monolayer in the same temperature range.

As with reaction rate, the mechanism of ozonolysis has been shown to depend on the characteristics of the surface. Enami *et al.* performed a series of studies that employed electrospray mass spectrometry to investigate ozonolysis of aqueous microdroplets of several organic compounds including uric acid,[84] ascorbic acid,[85] sulfonic acid,[86] phenol and α-tocopherol,[87] cysteine,[88] and β-caryophyllene.[89] After identifying unique products from these reactions that were distinct from those in the bulk solution, they concluded that an air–water shell a few nanometers thick presents a reaction environment that is fundamentally different from that found in the bulk.

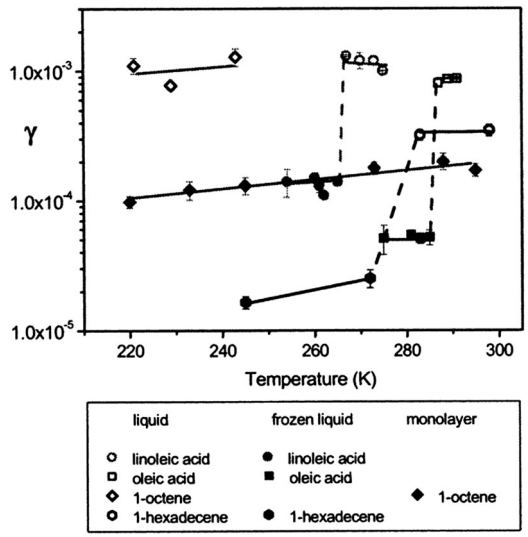

Fig. 4 Ozone reactive uptake coefficients, γ, *vs.* temperature (K) for several organic liquids, frozen liquids, and a monolayer.[82,83] The dashed lines show an order of magnitude difference in uptake coefficient between liquid and frozen samples. Reprinted (adapted) with permission from *J. Phys. Chem. A*, 2002, **106**, 6469–6476. Copyright 2002 American Chemical Society.

They showed, specifically in β-caryophyllene ozonolysis, that different products were formed at different depths within this shell, in correlation with varying water densities. As the water density changes, the rate of vibrational relaxation changes as well, allowing for the activation of different processes.[89] To further elucidate the role of water molecules at the interface, Beauchamp and coworkers[90] investigated the ozonolysis of phospholipid surfactant mixtures using field-induced droplet ionization mass spectrometry. They found known metastable species in the bulk as major products of ozonolysis at the air–water interface. Lower water density at the interface relative to the bulk may play a key role, as proton transfer from water leads to rapid decomposition of these products. Also, as found in the study of ozone exposure to naphthalene on water droplets by Raja and Valsaraj,[79] ozonolysis of unsaturated reactants resulted in increased molecular hydrophilicity, leading to dissolution of products into the aqueous phase. Most recently, Beauchamp and coworkers have developed a method for generating controlled nanoliter-sized droplets for mass-spectrometric sampling using bursting bubble ionization and interfacial sampling with an acoustic transducer.[91] This method has been used to investigate the time-dependent ozonolysis of oleic acid.

Investigations of the heterogeneous ozonolysis of oleic acid have more recently been expanded to include macroscopic surface samples.[82,92] For example, flow-tube methods have been used to examine interfacial reactions of oleic acid on a variety of substrates.[71,82,92] Further, ATR-IR has been utilized to monitor oxidation at the interface of large and small oleic acid droplets.[93] The reactive uptake coefficients measured for extended surfaces were found to range from 10^{-5} to 10^{-3}, depending on experimental technique, sample geometry, the influence of secondary reactions,[93] and whether the coefficient was calculated using changes in O_3[92] or in oleic acid concentrations or properties.[82,93] Additionally, Reid and coworkers investigated oxidative aging of aerosol particles containing environmentally relevant organic acids using optical tweezers and cavity enhanced ringdown spectroscopy.[94,95] For mixed NaCl/oleic acid particles, they report an uptake coefficient of 2.3×10^{-4}, which is consistent with measurements cited above that employed ATR-IR experiments.[82,92,93] In another droplet-based study, O_3 reactions with oleic acid surfaces were investigated through the use of a pendant drop of water coated with a monolayer of oleic acid.[96] The authors attributed a relatively low uptake coefficient ($(2.6 \pm 0.1) \times 10^{-6}$) to the decrease in accessibility of ozone to the C=C bond, which was submerged within the oleic acid monolayer (Fig. 5).[42]

From a much more fundamental perspective, studies employing self-assembled monolayers (SAMs) as model surfaces have provided detailed insight into the dynamics of gas–surface collisions involving ozone. Specifically, dynamic properties including energy transfer and thermal accommodation coefficients, as well as reaction probability of a single surface-bound functional group, have been revealed using SAMs. These surfaces present many advantages for fundamental work: they can be synthesized in a highly reproducible manner, they can be characterized *in situ* with infrared spectroscopic probes, and they enable one to locate a specific functional group precisely at the gas–surface interface. With this strategy, Dubkowski *et al.*[97] and Vieceli *et al.*[98] employed time-resolved changes in atmospheric-pressure ATR-IR band intensities as well as molecular dynamics simulations of alkene-terminated SAMs to describe the interaction of O_3 with a SAM. Their experimental results suggested a surprisingly long surface residence time for ozone: ~7 s, which was many orders of magnitude longer that that shown by their simulations: ~17 ps. As nonreactive molecular dynamics were used in the simulations, the vast difference in residence time was attributed to the formation of covalent bonds initially leading to the primary ozonide in the experiment, which was not modeled in the simulations. The simulations also showed

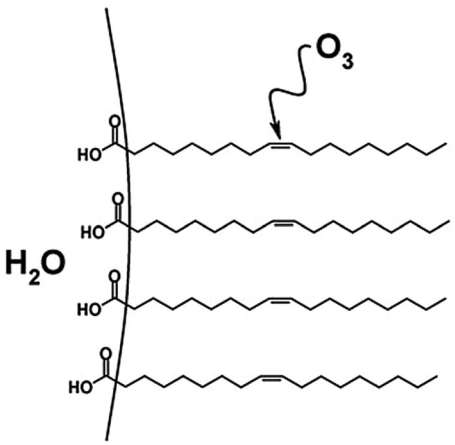

Fig. 5 An oleic acid monolayer on a pendant drop of water. The non-terminal positioning of the C=C double bond hinders reaction with O_3, resulting in a decreased reactive uptake relative to a monolayer with a terminal C=C bond. Reproduced from ref. 42 with permission from the PCCP Owner Societies.

that (possibly reactive) collisions of O_3 with C=C double bonds in organic systems were dependent upon the residence time of ozone on the organic surface before desorption, as well as the accessibility of unsaturated sites within the organic surface to ozone.[98] Specifically, the ozone collision probability with C=C bonds was found to be a factor of two lower for a vinyl-terminated SAM than for a liquid slab of 1-tetradecene. In the SAM, the C=C bonds are located at the gas–surface interface, allowing access to ozone without uptake into the organic phase. However, a shorter residence time on the SAM (17 ps) than in the liquid (53 ps) leads to an overall lower collision probability. Further, for a phospholipid monolayer surface with submerged C=C bonds, this probability decreased by a factor of five relative to the SAM. Though ozone had a similar residence time on the phospholipid surface (51 ps) as on the liquid, the localization of the C=C double bonds beneath the gas–surface interface hindered accessibility to ozone as compared to the SAM, or to the liquid, which had C=C bonds dispersed evenly throughout.

To gain insight into the fate of vinyl-functionalized organic surfaces upon reaction with ozone, McIntire *et al.*[99] obtained AFM and SEM images, as well as Auger spectra of a model surface (vinyl-terminated SAM on silicon) following exposure to ozone in a Teflon reaction chamber. Their AFM data, shown in Fig. 6, displays images of a silicon substrate before and after deposition of the SAM, as well as after ozone oxidation, at both low and high relative humidity. At low relative humidity, Criegee intermediates (CI) decompose or react with adjacent organic species (Fig. 6e). Subsequent reactions of these products ultimately lead to radical-induced polymerization of the SAM chains into the aggregates shown in Fig. 6c (white). In contrast to these interesting structures, high relative humidity appears to provide competing reaction pathways that limit the degree of agglomeration (Fig. 6d).

While SAMs provide well-characterized model organic surfaces for fundamental studies of interfacial ozone chemistry, vacuum-based molecular beam methods enable one to also

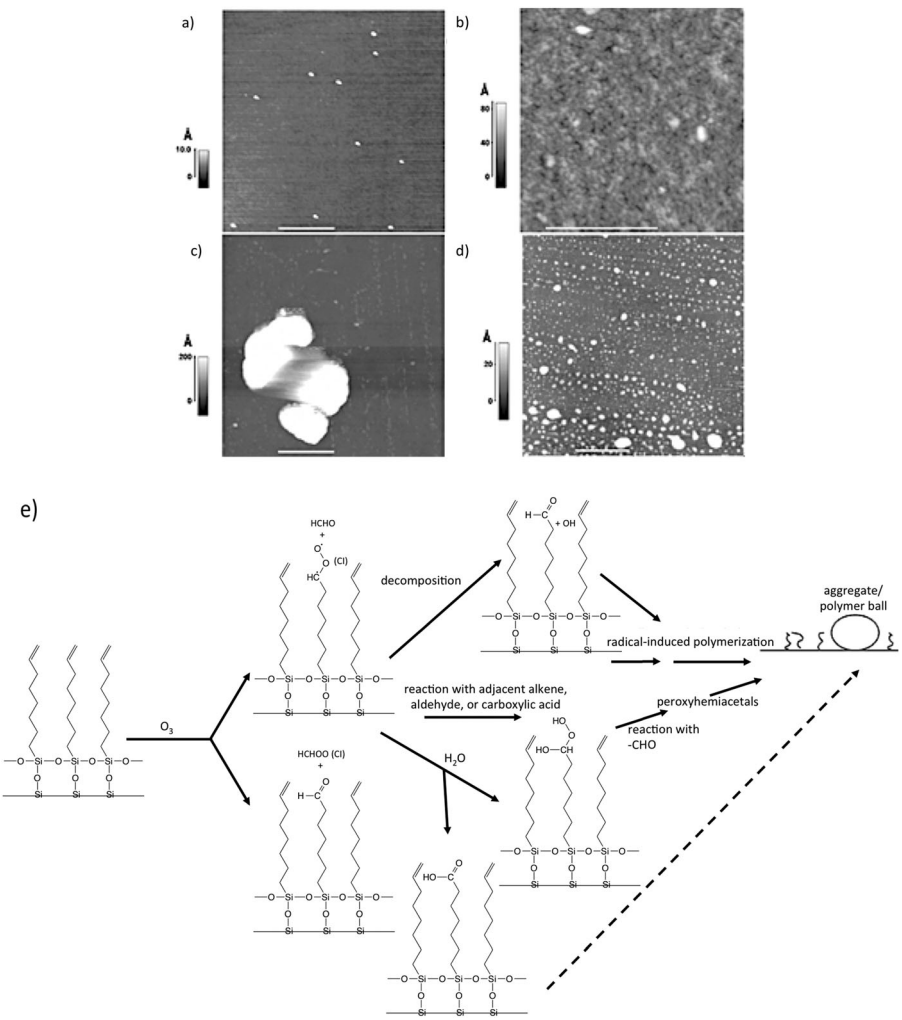

Fig. 6 AFM images of a clean Si substrate (a) before deposition of a vinyl-terminated SAM. Small particles of silica shown result from surface "chipping" during handling; (b) following deposition of SAM; (c) following exposure to ozone for 40 min at <5% relative humidity; (d) same as in (c), but at 60% relative humidity; (e) scheme showing reactions of Criegee Intermediates leading to radical-induced polymerization. Reproduced and adapted from ref. 99 with permission from the PCCP Owner Societies.

precisely control the properties of the impinging gas molecules. Ultra-high vacuum (UHV) approaches, in particular, virtually eliminate the participation of background gases in the surface chemistry. Although the UHV-based measurements are not immediately relevant to reactions that take place under atmospheric conditions, they do provide valuable benchmarks for theoretical studies of these reactions, aid in spectral assignments of interfacial functional groups, and reveal how O_3 reacts with organic surfaces under pristine conditions. Such experiments are the first steps in building a more comprehensive understanding of these reactions.

Lu, Fiegland, and coworkers[100–102] have combined SAMs, UHV, and molecular beam scattering methods to explore the dynamics of surface-bound functional group oxidation during collisions with ozone molecules. Using time-of-flight methods, they found bimodal energy distributions for ozone scattered from methyl-, hydroxyl-, and perfluoro-terminated SAMs.[102] One mode of the energy distribution was attributed to those molecules that transferred sufficient energy to the surface upon collision to become transiently trapped where they are unable to immediately surmount the energy barrier for desorption. Eventually, the thermal energy of the surface drives desorption of this fraction of ozone molecules, which exhibit a Boltzmann distribution of final velocities. The remaining component of the scattering distribution was attributed to those molecules with sufficient energy to scatter impulsively from the surface upon collision without becoming fully accommodated. By comparing the incident and final energies of molecules, the extent of energy transfer to the surface upon collision was deduced. For the methyl-terminated SAM, extensive energy transfer evidenced by a dominant Boltzmann component was attributed to the large number of low-energy degrees of freedom that efficiently absorb ozone's translational energy. Interestingly, ozone scattering from the hydroxyl-terminated SAM, which displays increased rigidity due to hydrogen bonding amongst terminal groups, resulted in a Boltzmann component similar to the one obtained with the methyl-terminated SAM. The authors suggested that a relatively strong gas–surface attractive potential plays a major role in bringing ozone to thermal equilibration on the more rigid hydroxyl-terminated SAM. Conversely, the perfluoro-terminated SAM possesses both high rigidity and weak gas–surface interactions that lead to a much smaller Boltzmann component to the final energy distribution and relatively low overall energy transfer from the gas to the surface.

More recently, molecular beam scattering methods, together with *in situ* monitoring of surface functional groups *via* RAIRS, have been employed to explore the reaction dynamics of ozone during exposure to a vinyl-terminated SAM in UHV. Results from the molecular beam scattering experiments support a mechanism that involves extensive thermal accommodation, especially at low beam energies, followed by inter-chain anhydride group formation.[101] Importantly, the initial reaction probability for ozone incident energies near room temperature was found to be 1.1×10^{-5}.[100] Finally, the effect of ozone translational energy on the reaction probability was also investigated in this experimental study. The results suggest that accommodation of ozone on the surface is required prior to reaction for room-temperature translational energies; however, at higher incident energies, a direct reaction driven by the beam energy appears to occur.[100] As shown in Fig. 7, this change of mechanism is evidenced by an increase in the initial reaction probability with incident energy.

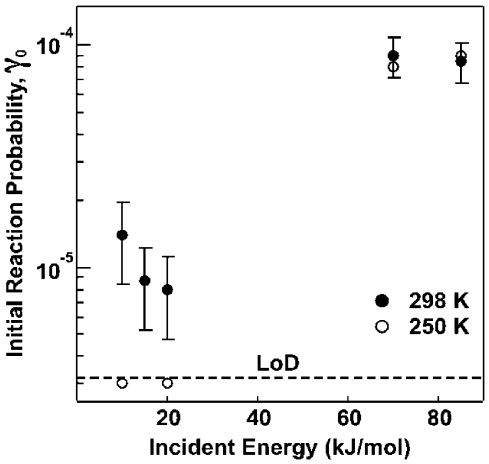

Fig. 7 Initial reaction probability for O_3 impinging on a vinyl-terminated self-assembled monolayer as a function of collision energy and surface temperature. Error bars represent one standard deviation. Reprinted with permission from *J. Phys. Chem. C*, 2011, **115**(51), 25348. Copyright 2011 American Chemical Society.

An interesting result stemming from these UHV experiments is that the reaction probability measured in the UHV-based molecular beam experiments (for thermal energies) is surprisingly similar to those found in an ambient environment, even though the reaction conditions are significantly different. To reconcile these findings, a comparison of the microscopic mechanisms of the gas–surface collisions in both types of experiments is required. When ozone collides with the SAM, it can impulsively scatter from the surface or become trapped onto the surface. Once trapped, an accommodated ozone molecule can diffuse along the surface until it either reacts or desorbs. In an ultra-high vacuum environment, once an adsorbed molecule surmounts the trapping potential, it desorbs irreversibly, as the likelihood of encountering another gas-phase molecule and becoming deflected back to the surface is very low. At atmospheric pressures, the desorbing gas molecule might be reflected back to the surface by other gases present in the environment, which would make the reaction probability higher than in UHV conditions. The reaction probability is similar under both sets of conditions likely because the ordered nature of the SAM used in UHV environment facilitates reactions in a manner that does not occur within other, less ordered surfaces used in the investigations under atmospheric conditions. Thus, an opportunity for further work in this area exists, as one may explore similar systems under atmospheric conditions or investigate the role of monolayer order, chain tilt, and packing density on the overall chemistry.

III. NO_3 reactions with organic surfaces

As with ozone, many of the studies of heterogeneous reactions of organics with nitrate radicals have involved the deposition of liquid[37] and solid[37,39,103–105] organic substrates onto flow tube reactors. Subsequent product analysis typically employs mass spectrometry, though alternative methods of detection have been used.[37]

One representative study by Knopf *et al.* investigated the effect of relative humidity on the uptake of NO_3 radicals on aerosols generated during biomass burning.[103] By varying the length of the flow tube and therefore the exposure area of the substrate, they determined first-order NO_3 loss rate constants, which they subsequently used to calculate NO_3 uptake coefficients. Further, using insights from proposed reaction mechanisms and physical properties of substrate molecules such as vapor pressure, they explained differences in NO_3 uptake behavior as a function of NO_3 exposure. In the presence of O_2, reactive uptake coefficients were found to be in the range of $1–26 \times 10^{-3}$. Other groups have investigated the reactive uptake coefficients of NO_3 (both in the presence and absence of O_2) on organic aerosols using flow tube reactors, and the reported uptake coefficients were also within this range.[37,104] Conversely, additional work, using similar methods, have measured NO_3 uptake coefficients up to two orders of magnitude larger.[39,105] Variances in the measured uptake coefficients may be attributed to differences in the linear flow velocities employed in different laboratories or differences in surface composition and preparation conditions.

In a comparison of liquid-phase and solid-phase deposition, Moise and coworkers[37] reported a decrease of the uptake coefficients by as much as a factor of five upon freezing for some organics (*i.e.*, *n*-hexadecane and *n*-octanoic acid) and no change for others (*e.g.*, 1-hexadecene, 2,2,4,4,6,8,8 heptamethyl nonane, and 10,12 octadecadienoic acid). For the reactions in which the coefficient did not change upon freezing, evaporation or mobility of the surface molecules was thought to provide a constantly renewed surface. The authors related key differences in these surface mechanisms to the solubility constant and diffuso-reactive length ("the approximate distance within the liquid over which reaction is taking place",[106] calculated using the ratio of the diffusion coefficient to the first-order loss rate) of NO_3 in each liquid organic.

To more completely describe the reactive uptake coefficient of NO_3 at substrates investigated by Knopf *et al.*,[103] Shiraiwa *et al.* used computational kinetic flux models to quantify the relative role of surface and bulk reactions for highly functionalized organic molecules relevant to biomass burning.[107,108] More specifically, by relating uptake coefficients to bulk accommodation coefficients (*i.e.*, the probability of a gas molecule colliding with the surface to enter the bulk of the particle), the contribution of surface reaction to the overall reaction was revealed to be dependent on the mechanism of reaction. For example, surface contributions were minor for levoglucosan, which reacts with NO_3 *via* an initial hydrogen-abstraction step—a relatively slow process. On the other hand, for abietic acid, which can react with NO_3 *via* relatively rapid addition across a double bond, surface contributions dominate. Further, desorption lifetimes and bulk diffusion coefficients of NO_3 into these organic surfaces were also determined.[38]

To complement the studies of NO_3 reaction with organic molecules deposited on surfaces, Schütze and Hermann[109] investigated the uptake of nitrate radicals into single drops of an aqueous solution of an organic dye inside a flow-tube reactor. A change in absorbance of the dye solution brought about by reaction with nitrate radicals allowed for the *in situ* determination of the reactive uptake coefficient of NO_3 radicals using UV-Vis spectroscopy. Falling within the range of values reported in studies by Knopf *et al.*[103] and others,[37,104] the uptake coefficient was found to be $(2.7 \pm 0.8) \times 10^{-3}$.[109]

Aside from experimental approaches that involve the direct deposition of substrates onto the surface of a flow tube, heterogeneous reactions of NO_3 with organic surfaces have been examined using particles/aerosols with organic compounds adsorbed on them. Organic molecules ranging from simple polycyclic aromatic compounds[110] to more complex organophosphorus pesticide molecules[111,112] have been deposited at the surface of azelaic acid for the study of nitrate radical reaction rates and mechanisms. Many of these studies have employed mass spectrometry coupled with gas chromatography to help characterize gas-phase product and reactant concentrations. Typical uptake coefficients obtained in this manner lie within the same range determined from the afore-described flow-tube deposition studies, thereby helping to validate the flow-tube approach as a viable means by which to explore the type of chemistry that occurs on aerosol particles.

Beyond aerosol and liquid flow-tube experiments, model organic molecular substrates have proven to be valuable tools in the study of nitrate radical reaction pathways. Bertram and coworkers, for example, studied the reactions of nitrate radicals with alkane- and alkenethiol self-assembled monolayers on gold substrates in a flow-tube reactor arrangement.[113,114] The reactive uptake coefficients they determined were 8.8×10^{-4} for an alkane monolayer and 3.4×10^{-2} for an alkene-terminated monolayer. A similar variation in coefficients was found when they compared other alkane and alkene systems. Differences in the reactive uptake coefficients found by the Bertram group from those obtained in previous studies of NO_3 chemistry[37,103,104] may be due to the greater accessibility of the double bond to NO_3 radicals in the monolayer studies. In a separate study,[105] Bertram and coworkers suggest that NO_3, like O_3, interacts with atmospheric surfaces through the Langmuir–Hinshelwood mechanism, though a complete description of the overall reaction mechanism has yet to be developed.

In addition to the measurements of reaction rates by Bertram and coworkers, the mechanism of reaction between these monolayers and nitrate radicals was explored using time-of-flight mass spectrometry to detect gas-phase products, while XPS and infrared spectroscopy were employed to analyze the surface-bound molecules following exposure.[114] The reaction was conducted in the presence of atmospheric gases that may have interfered with the reaction of pure NO_3 with the surface.

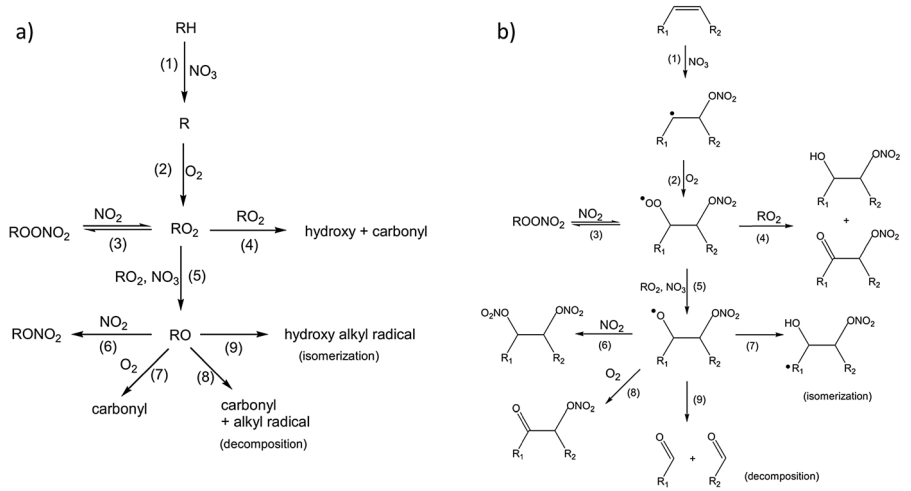

Fig. 8 Proposed mechanism for addition of NO_3 to an (a) alkane and (b) alkene surface in the presence of NO_2 and O_2. Copyright 2009 Wiley. Used with permission from S. Gross and A. K. Bertram, *Products and kinetics of the reactions of an alkane monolayer and a terminal alkene monolayer with NO_3 radicals*, *J. Geophys. Res.: Atmos.*, 2009, **114**, D02307.

In fact, background O_2 and NO_2 are critical co-reactants in the mechanisms proposed by Bertram *et al.* As shown in Fig. 8, nitrate initially abstracts a hydrogen atom from alkanes (Fig. 8a), or adds to one side of the C=C bond in alkenes (Fig. 8b), leaving in a radical site for subsequent O_2 addition and further reactions with other oxidative species.

In an effort to explore the interfacial chemistry of nitrate radicals at organic surfaces in the absence of background gases and other possible contaminants, Zhang *et al.*[115] explored these reactions at the surface of an alkenethiol self-assembled monolayer in the highly regulated environment of a UHV chamber. Additionally, the use of *in situ* reflection–absorption infrared spectroscopy (RAIRS) in their work allowed for the characterization of the surface during the course of nitrate radical exposure, thereby enabling an in-depth study of the reaction kinetics. The majority of studies prior to this work presented reactive uptake coefficients with little-to-no direct tracking of chemical bond breaking and formation at the surface. By directly monitoring changes in the infrared band intensity of the stretching mode associated with the surface carbon–carbon double bonds, Zhang *et al.* reported an initial reaction probability of $(2.3 \pm 0.5) \times 10^{-3}$. This investigation was complemented by a quantum/molecular mechanical computational study that facilitated the identification of intermediates and products as well as the elucidation of a reaction mechanism from vibrational spectra. As shown in Fig. 9, a mechanism was proposed wherein NO_3 adds to the C=C double bond resulting in the formation of an alkyl nitrate radical. Electronic structure calculations revealed that hydrogen abstraction from the terminal carbon atom could be deemed unlikely under the thermal conditions of the experiment, as only a very small fraction of NO_3 molecules had enough energy to overcome the calculated abstraction barrier. Notably, this is the first study of the reactions involving NO_3 and organic surfaces to incorporate gas collision energy into a discussion of reaction mechanisms.

The synergistic link between the work performed under atmospheric pressure by Bertram and coworkers and that of Zhang *et al.* is that both studies suggest that the first step in the reaction is the generation of a surface-bound radical. This step defines the initial reaction probability for NO_3 at vinyl-terminated surfaces and appears to be uninfluenced by background gases. Therefore, computational studies that approach this problem in the absence of background contamination are likely appropriate approaches for exploring the fundamental energetics of the first steps in the reaction. Once the surface-bound radicals are formed, background gases likely play a major role in scavenging the radicals and further oxidizing the surface. The next step in both types of studies must be to increase the complexity of the

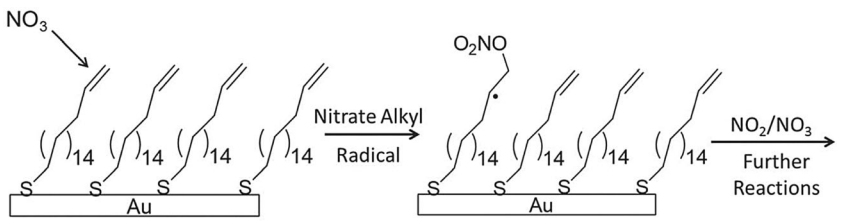

Fig. 9 A scheme for the reaction of nitrate radical with a vinyl-terminated self-assembled monolayer. Positioning of the C=C bond at the gas–surface interface affords a higher reaction probability than in experiments with a submerged C=C bond (as shown in Fig. 5 for O_3 reactions). Reproduced from ref. 115 with permission from the PCCP Owner Societies.

systems to better model heterogeneous atmospheric chemistry by including highly defective surfaces and the presence of critical co-reactants within the surfaces as well as within the gas phase.

IV. OH reactions with organic surfaces

Reactions with hydroxyl radicals alter the fate and properties of atmospheric organic particles. Moreover, heterogeneous OH chemistry affects the atmospheric concentrations of ozone and nitrate. A distinctive aspect of this oxidant is that its high reactivity makes it difficult to quantify its concentration, and therefore, quantitative experiments are not as well developed as for ozone and nitrate. Nonetheless, as with ozone and nitrate gases, studies of hydroxyl radical heterogeneous chemistry have been performed largely with the use of flow reactor tubes coupled to mass spectrometric product identification methods. In many of these studies, squalane (a long, branched liquid alkane at ambient conditions[20]) has been employed as the liquid of choice to model the surface of ambient aerosol particles.

In one such study, Smith *et al.*[116] generated hydroxyl radicals from O_3 photolysis in the presence of H_2O in a flow tube containing deposited particles of squalane, and they monitored the composition of aerosol particles leaving the tube with a custom-built aerosol mass spectrometer. A relative-rate method employing the loss of particle-phase squalane over the course of OH exposure was used to determine a reactive uptake coefficient of 0.3 ± 0.07. As expected from previous work,[1,117,118] the reactive uptake coefficient was found to be several orders of magnitude above that for either ozone or nitrate radicals—a consequence of the relatively high chemical potential of the hydroxyl radical and small (or nonexistent) barrier for hydrogen abstraction.[119,120] Interestingly, the coefficient is still over a factor of three lower than unity, which indicates that 70% of the OH molecules escape the gas-squalane collision without reaction. Those molecules either impulsively scatter without mass accommodation or trap on the surface but desorb prior to achieving a particular orientation leading to reaction. The authors proposed reaction mechanisms that depend on OH exposure. At low exposures, sequential oxidation predominates, yet at higher, atmospherically relevant exposures, volatilization into various gas-phase functionalized organic products prevails. In other words, there is a competition between oxidation and surface mass loss that changes with time.

In another experiment, aimed at correlating the structure and phase of an organic aerosol to its reactivity, Ruehl *et al.*[121] also used a photo-oxidation flow-tube method coupled to GC/MS analytical methods. They measured a reactive uptake coefficient similar to that described above for squalane (0.36 ± 0.11), which they found to be higher than that for octacosane (0.18 ± 0.11), a normal alkane with a slightly smaller molecular weight. The difference in coefficients between the two molecules is not only due to differences in structure (*i.e.*, branched *vs.* straight chain), but also to differences in phase. Octacosane is a solid at room temperature; therefore, the diffusion of unreacted organic molecules from the bulk to the surface is much slower than in a liquid. Moreover, the authors confirmed a "surface freezing" phenomenon in which linear alkane molecules were preferentially oriented normal to the surface. They substantiated this claim with a positional distribution of functionalized octacosane products, showing a higher probability for functionalized products near the terminus of the octacosane backbone (Fig. 10), as this region is most accessible to OH exposure. As with the study by Smith *et al.*,[116] Ruehl *et al.* propose a higher likelihood of functionalization at shorter oxidation lifetimes and fragmentation leading to carbon loss at longer lifetimes.

Che *et al.*[20] also investigated the reaction between hydroxyl radicals and squalane aerosols in an experiment that showcased a novel method in which the heterogeneous chemistry of organic aerosols was studied in a continuous-flow stirred tank reactor in place of a stationary flow-tube reactor. This modification affords long-term stable reaction conditions. With this method, a larger reactive uptake coefficient (0.51 ± 0.10) for squalane exposure to OH radicals was reported. The authors attribute the difference between this uptake coefficient and that obtained in the study by Smith *et al.*[116] to the influence of secondary chemistry (more than one squalane molecule may

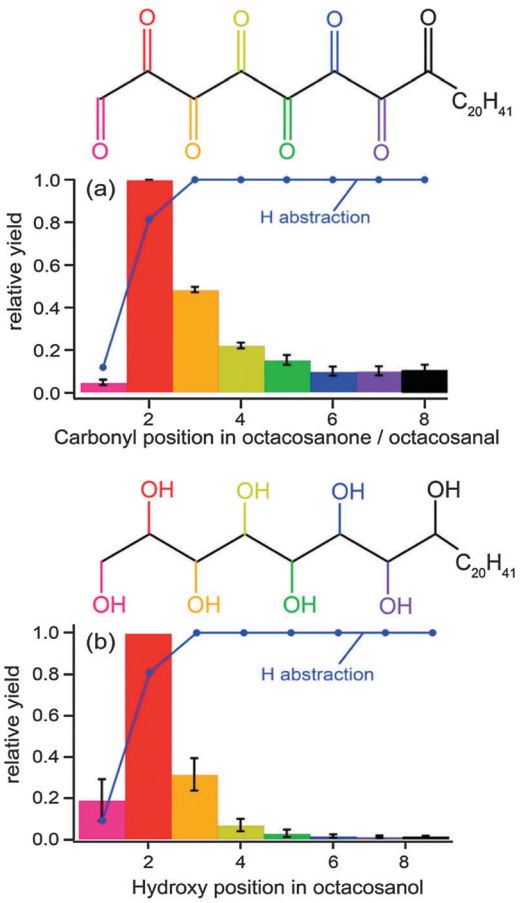

Fig. 10 Preferential positioning of ketone and alcohol groups resulting from the functionalization of octacosane by OH exposure suggests a "surface freezing" phenomenon. Reprinted (adapted) with permission from *J. Phys. Chem. A*, 2013, **117**, 3990. Copyright 2013 American Chemical Society.

react per OH), which is a pathway that their approach may be more sensitive to than the stationary flow-tube method.

To gain more insight into the extent of secondary chemistry of OH with organic aerosols, Kolesar *et al.* investigated the effect of exposing a squalane seed coated with viscous SOA material (a product of α-pinene ozonolysis) to OH in a flow tube.[122] The presence of the SOA coating enhanced squalane loss. The authors hypothesized the formation of radicals at the particle surface that are able to migrate through the SOA matrix to the squalane support where further reactions occur.

Flow-tube studies of heterogeneous reactions of hydroxyl radicals with organic aerosols ranging from those present in soot[50,117,123–125] and biomass-burning aerosols,[126–128] to those from herbicides,[129] pesticides,[130,131] and flame retardants,[132,133] have been performed to obtain information such as product structure,[117,123,125,130,134] yield and volatilization,[123,126] changes in hygroscopic properties[124] and particle size,[124,131] as well as kinetic information such as reactive and degradative rate constants[50,126,127,129–134] and reactive uptake coefficients.[50,117,125,126,132,135] These reactive uptake coefficients are generally large, but vary significantly between 0.19 and 2.0,[50,117,132,135] although even higher values have been reported.[125] It should be noted that values above 1.0 are only possible for those coefficients determined by measuring particle loss[117,125,132,135] as opposed to OH loss.[126] That is, secondary reactions, such as propagation steps in radical polymerization may result in the elimination of multiple particles for a single OH radical.[117,125,135,136] Small variations in uptake coefficient have also been attributed to differences in parametric fit of loss data, presence of O_2 in the reaction environment, and variations in the kinetic energy of OH.[116]

Recently, flow-tube studies by Wilson and coworkers have added insight into the role of molecular structure and O_2 concentration on the mechanism of organic aerosol oxidation by OH.[137,138] Using mass-spectrometric data, this group compared the reaction mechanisms for both branched squalene and linear linonenic acid (Fig. 11). Both reactions were found to be initiated by the addition of an OH radical to a C=C double bond to yield a hydroxyalkyl radical. O_2 was found to add to this radical, which results in the formation of a hydroxyperoxy moiety. In reactions with squalene (Fig. 11a), the OH radical adds to the less substituted carbon, leading to a tertiary hydroxyperoxy radical. This radical has no adjacent hydrogens with which to self-react, which preferentially leads to the production of a hydroxyalkoxy radical (A6) over a diol (A5). The hydroxyalkoxy radical may then dissociate (A7) to form a variety of fragmentation products. In the absence of O_2, hydrogen abstraction (A2) or subsequent OH radical addition (A3) after the initiation step leads to a variety of products. Thus, at lower O_2 concentrations (~1% in this study), "functionalization products" dominate, and at higher O_2 concentrations (~10% in this study), "fragmentation products" dominate. Conversely, in reactions with linolenic acid (Fig. 11b), a secondary hydroxyperoxy is available to react with an adjacent hydrogen atom (B6), favoring functionalized product formation over hydroxyalkoxy formation (B7). At both O_2 concentrations used in this study, functionalization products dominate for the linolenic acid reaction. The Wilson group has also developed and experimentally validated a theoretical model for the reaction of squalane with OH radicals.[48] As such, they related the uptake coefficient to the gas-phase OH density and the size and materials properties of the aerosol.

Beyond aerosol studies, larger-scale surfaces have provided insight into the heterogeneous chemistry of OH. In a laboratory study by Bertram *et al.*,[139] several surfaces including waxes, methyl- and vinyl- self-assembled monolayers, pyrene, and soot were deposited on the inside wall of a Pyrex flow tube as a proxy for suspended particles in the atmosphere. The reactive uptake coefficient in the Bertram work (determined *via* hydroxyl loss, as in the study by Slade *et al.*[126]), ranged from $(6 \pm 3) \times 10^{-4}$ for halocarbon wax to 0.88 ± 0.38 (with an upper limit of 1) for soot.

In an effort to provide insight into the role of surface properties in the interaction between hydroxyl radicals and surface-adsorbed organics, Iuga *et al.* used density functional theory methods to explore the potential energy of the reaction between a hydroxyl radical and formaldehyde bound to the monomer $Si(OH)_4$[140] and small silicate polymers.[141] In these studies, reaction pathways, along with rate constants and energy

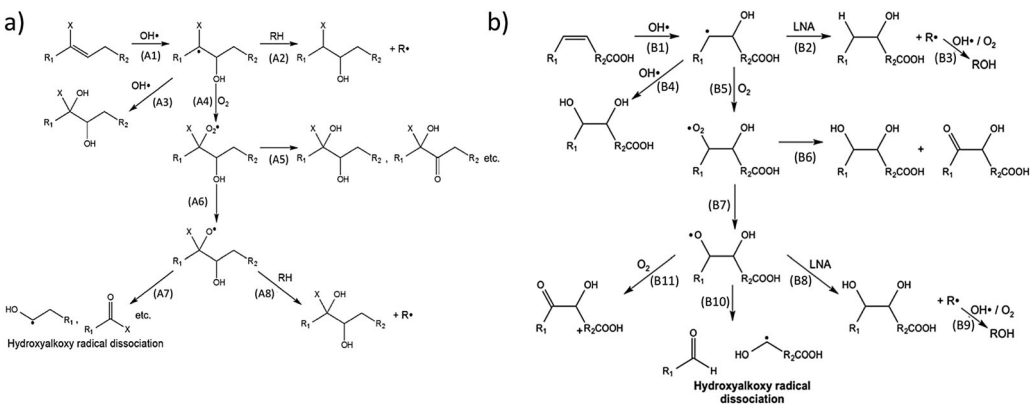

Fig. 11 Proposed mechanism for addition of OH to (a) squalene, a branched alkane, and (b) linolenic acid, a linear, unsaturated carboxylic acid, in the presence of O_2. Reprinted (adapted) with permission from (a) *J. Phys. Chem. A*, 2014, **118**, 4106. (b) *J. Phys. Chem. A*, 2014, **118**, 11555. Copyright 2014 American Chemical Society.

profiles, were generated for several possible mechanisms. A notable result of this theoretical work is that the OH—formaldehyde reaction yielded a lower rate constant in the presence of dust (*i.e.*, silicates) than in the gas phase, thus suggesting that surface-adsorbed molecules may not be as reactive to OH as they are in the gas phase. This difference likely stems from the obstruction of particular reactive approach geometries for the OH + formaldehyde pair on the surface relative to the gas phase.

Further key information about OH surface chemistry emerged from the work of Dilbeck and Finlayson-Pitts,[142] who studied the reaction between hydroxyl radicals and both saturated and unsaturated phospholipid molecules adsorbed onto an NaCl surface in the presence of O_2. Infrared-spectroscopic measurements recorded during OH exposure, in conjunction with MALDI-ToF mass spectrometric measurements, were used to identify product functional groups. Further, changes in IR bands were used to determine the loss rate of specific vibrational modes during the gas–surface reaction. Consequently, probabilities for reaction at specific sites on the organic molecule could be obtained. With these methods, the scientists determined a reaction probability of $(4 \pm 1) \times 10^{-3}$ for OH radical addition to the C=C double bond of the unsaturated phospholipid surface molecules and a hydrogen abstraction probability of $(8 \pm 1) \times 10^{-4}$ from the methylene groups of the saturated surface. The authors suggest that the surprisingly low measured probabilities may be attributed to phospholipid aggregation during sample preparation, thus restricting the availability of surface molecules for reaction. Hence, the values reported here are likely only lower limits.

The importance of functional group accessibility was exemplified in follow-up work by Moussa and Finlayson-Pitts[143] that utilized ATR-IR to investigate the reaction of OH radicals with unsaturated self-assembled monolayers (in the presence of O_2). In that work, infrared spectra were recorded during OH exposure and analyzed to provide a reaction probability of 1.1 ± 0.9 for addition of OH to the C=C double bond. These measurements clearly showed that vinyl groups positioned precisely at the gas–surface interface are extremely reactive toward hydroxyl radicals and that their lifetime is directly related to the gas-phase OH concentration. Furthermore, the unit reaction probability indicates that every OH molecule, regardless of impact parameter, orientation, or translational energy, reacts with the surface, which is fundamentally different from interfacial reactions involving the nitrate radical or ozone (*vide supra*).

In another thin film study, Mysak *et al.*[144] used XPS to investigate the reaction of hydroxyl radicals with coronene on a single-crystal metallic substrate in ultra-high vacuum. These measurements allowed for the examination of changes in film thickness as well as functional group distribution as a function of reaction time. The authors found that there is an increase in the surface oxygen-to-carbon ratio over the course of a heterogeneous OH reaction that is controlled by the formation of oxygenated functional groups as well as through carbon loss, as described in prior work.[20,116,138] To help explain the increase in oxygen-to-carbon surface ratio with reaction time, Mysak *et al.* proposed that the initial transformation of reduced organic aerosols occurs *via* a different pathway (functionalization) than that of the highly oxidized aerosols (carbon loss), which is consistent with chemistry described in previous flow-tube type studies.[116,121]

Highly fundamental investigations have helped to shed significantly more light on these reaction pathways. Two key studies by the McKendrick group have implemented laser-induced fluorescence techniques *in vacuo* to probe the collision dynamics between hydroxyl radicals and liquid organic thin films of squalane. In the first published study,[145] the objective was to examine a novel photolytic source of hydroxyl radicals and determine the contributions of impulsive scattering and thermal desorption mechanisms to the final energy distribution of OH radicals scattered from the surface. Separate trajectory calculations complemented this work by revealing the importance of the impulsive scattering and thermal desorption in collisions of OH with a perfluorinated SAM surface.[146] In the second study,[147] a broader range of liquids (squalane, squalene, and oleic acid) was examined with the same techniques. The reactive uptake coefficients (determined *via* OH loss) were found to be between 0.24 ± 0.10 (oleic acid) and 0.39 ± 0.10 (squalane). Interestingly, these values are similar to those determined for the analogous reactions at particulates.[121]

In other key studies, McKendrick and coworkers scattered OH radicals from a non-reactive fluorinated surface and determined the contributions of impulsive scattering and thermal-desorption mechamisms in the desorbing OH flux.[148] The thermal-desorption fraction of the OH flux was then assumed to react following a Langmuir–Hinshelwood mechanism in experiments in which OH was aimed at reactive surfaces. Enami and coworkers further explored the idea of OH reactions undergoing a Langmuir–Hinshelwood mechanism using electrospray ionization mass spectrometry. Results from dosing aqueous carboxylic acid microjets with a stream of hydroxyl radicals led to a description of the mechanism that involves initial reactions precisely at the gas–surface interface. Importantly, they inferred from the extent of acid depletion during reaction, as well as from previous knowledge that OH radicals prefer interfacial layers over the bulk,[149] that there is always an excess of OH radicals available to react in the outermost interfacial layers. This trapped layer of radicals is consistent with the Langmuir–Hinshelwood mechanism.[150,151]

The fundamental nature of the OH + –C=C and $-CH_3$ surface reaction was further investigated by D'Andrea *et al.*[136] when they examined the reaction of OH radicals with alkane- and alkene-thiol self-assembled monolayers deposited on gold using molecular beam scattering methods in an UHV environment. Coupled with RAIRS, this experiment showed real-time changes in surface functionalization over the entire course of OH exposure (as opposed to after different, long-exposure times[143]), thus providing a more detailed spectroscopic picture of the progression of the reaction. Following examination of spectral changes during exposure, reaction mechanisms of OH with both self-assembled monolayers were proposed. Both mechanisms, as shown schematically in Fig. 12, highlight the possibility for radical-induced polymerization of the organic chains in the monolayer, thereby providing insight into the

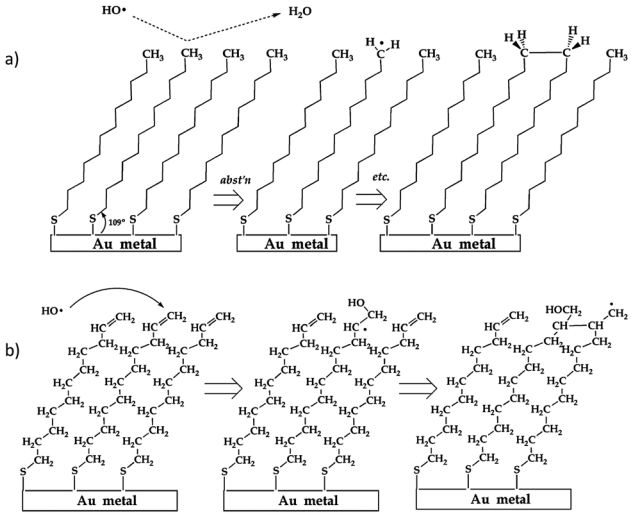

Fig. 12 Mechanisms of OH + (a) alkane and (b) alkene-terminated SAM surfaces proposed by D'Andrea *et al.* In (a), isolated alkyl radicals cannot diffuse due to SAM stability. Subsequent OH collisions can result in further radical generation and cross-linking dimerization. In (b), polymerization results in a cross-linked alcohol. Reprinted (adapted) with permission from *J. Phys. Chem. B*, 2008, **112**, 535. Copyright 2008 American Chemical Society.

secondary chemistry alluded to in previous studies (*i.e.*, where researchers reported reactive uptake coefficients greater than unity[117,125,132,135]).

V. Summary and perspectives

Oxidation by O_3, NO_3, and OH results in changes in the physical and chemical properties of organic particles and surfaces in the atmosphere. Importantly, these molecules functionalize initially hydrophobic organic particles rendering them hydrophilic, which dramatically affects their solubility in rain droplets, role as cloud condensation nuclei, and environmental transport. Moreover, changes in particulate size and composition affect the absorption and scattering of incoming sunlight. Consequences such as these have motivated scientists to study the interaction between highly oxidative pollutants and organic surfaces.

This review described the progress of research surrounding heterogeneous reactions of atmospheric oxidative gases and organic surfaces of atmospheric importance. A wide range of methods from flow tubes and mass spectrometry to molecular beam scattering and infrared spectroscopy have been used to inform scientists about kinetics and reaction mechanisms. Most recently, researchers have been challenged by the possibilities of polymerization initiated by radical-containing pollutants and further promoted by secondary mechanisms that do not directly involve the atmospheric initiator.

In addition to highly practical field measurements[152] and atmospheric sampling,[153] future research will continue to focus on deconstructing complex systems into their fundamental components and investigating real-time changes to organic surfaces during exposure to a controlled flux of gas-phase oxidants. In this way, scientists will independently study how key properties, such as gas-surface polarity, molecular structure, and density, affect the outcome of interfacial collisions.

Modern computational techniques will also continue to find a role in adding insight into the fundamental aspects of atmospheric heterogeneous chemistry. The same experimental systems that allow laboratory researchers to investigate individual components of complex atmospheric reactions readily lend themselves to *in silico* modeling. The uniform structure of model organic surfaces such as self-assembled monolayers allows for their facile computational modeling using quantum/molecular mechanical hybrid models as well as molecular dynamics techniques, which will provide great theoretical insight into oxidative processes on both the molecular and surface nanoscales.

As a result of investigations into heterogeneous chemistry and reaction dynamics of the atmospheric oxidants, O_3, NO_3, and OH, researchers are gaining insight into the role of surface structure and functionality in the reactions of these gases. While research in this field continues to progress, more will be learned about the effects of this chemistry on organic particulates and the balance of oxidative gas concentrations in the troposphere. Armed with this information, researchers will be able to make well-informed predictions about the fate of organics in the atmosphere as well as the impact of these oxidants on the environment.

Acknowledgements

The authors are grateful to Dr. Linsey Marr from the Virginia Tech Department of Civil and Environmental Engineering for her constructive comments on this work. This material is based upon work supported by, or in part by, the U. S. Army Research Laboratory and the U. S. Army Research Office under contract/grant number W911NF1410159.

References

1 R. Atkinson, *Atmos. Chem. Phys.*, 2003, **3**, 2233–2307.
2 D. Johnson and G. Marston, *Chem. Soc. Rev.*, 2008, **37**, 699–716.
3 R. Atkinson, *J. Phys. Chem. Ref. Data*, 1997, **26**, 215–290.
4 S. S. Brown and J. Stutz, *Chem. Soc. Rev.*, 2012, **41**, 6405–6447.
5 D. M. Etheridge, L. P. Steele, R. J. Francey and R. L. Langenfelds, *J. Geophys. Res.: Atmos.*, 1998, **103**, 15979–15993.
6 L. W. Richards, *J. Air Pollut. Control Assoc.*, 1988, **38**, 784–791.
7 M. C. Jacobson, H. C. Hansson, K. J. Noone and R. J. Charlson, *Rev. Geophys.*, 2000, **38**, 267–294.
8 B. T. Simoneit, *J. Atmos. Chem.*, 1989, **8**, 251–275.
9 L. J. Standley and B. R. T. Simoneit, *Environ. Sci. Technol.*, 1987, **21**, 163–169.
10 T. E. Graedel, D. T. Hawkins and L. D. Claxton, *Atmospheric chemical compounds: sources, occurrence and bioassay*, Elsevier, 1986.
11 D. J. Donaldson and D. Anderson, *J. Phys. Chem. A*, 1999, **103**, 871–876.
12 P. S. Gill, *Rev. Geophys.*, 1983, **21**, 903.

13 A. J. Tiwari and L. C. Marr, *J. Environ. Qual.*, 2010, **39**, 1883–1895.
14 M. Hallquist, J. C. Wenger, U. Baltensperger, Y. Rudich, D. Simpson, M. Claeys, J. Dommen, N. M. Donahue, C. George, A. H. Goldstein, J. F. Hamilton, H. Herrmann, T. Hoffmann, Y. Iinuma, M. Jang, M. E. Jenkin, J. L. Jimenez, A. Kiendler-Scharr, W. Maenhaut, G. McFiggans, T. F. Mentel, A. Monod, A. S. H. Prévôt, J. H. Seinfeld, J. D. Surratt, R. Szmigielski and J. Wildt, *Atmos. Chem. Phys.*, 2009, **9**, 5155–5236.
15 D. Schuetzle, D. Cronn, A. L. Crittenden and R. J. Charlson, *Environ. Sci. Technol.*, 1975, **9**, 838–845.
16 C. Fountoukis, A. G. Megaritis, K. Skyllakou, P. E. Charalampidis, C. Pilinis, H. A. C. Denier van der Gon, M. Crippa, F. Canonaco, C. Mohr, A. S. H. Prévôt, J. D. Allan, L. Poulain, T. Petäjä, P. Tiitta, S. Carbone, A. Kiendler-Scharr, E. Nemitz, C. O'Dowd, E. Swietlicki and S. N. Pandis, *Atmos. Chem. Phys.*, 2014, **14**, 9061–9076.
17 J. Jimenez, M. R. Canagaratna, N. M. Donahue, A. S. H. Prevot and Q. Zhang, *Science*, 2009, **326**, 1525–1529.
18 A. Virtanen, J. Joutsensaari, T. Koop, J. Kannosto, P. Yli-Pirila, J. Leskinen, J. M. Makela, J. K. Holopainen, U. Poschl, M. Kulmala, D. R. Worsnop and A. Laaksonen, *Nature*, 2010, **467**, 824–827.
19 B. J. Finlayson-Pitts and J. N. Pitts Jr, *Chemistry of the upper and lower atmosphere: theory, experiments, and applications*, Academic press, 1999.
20 D. L. Che, J. D. Smith, S. R. Leone, M. Ahmed and K. R. Wilson, *Phys. Chem. Chem. Phys.*, 2009, **11**, 7885–7895.
21 S. N. Chu, S. Sands, M. R. Tomasik, P. S. Lee and V. F. McNeill, *J. Am. Chem. Soc.*, 2010, **132**, 15968–15975.
22 R. S. Disselkamp, M. A. Carpenter, J. P. Cowin, C. M. Berkowitz, E. G. Chapman, R. A. Zaveri and N. S. Laulainen, *J. Geophys. Res.: Atmos.*, 2000, **105**, 9767–9771.
23 J. L. Fry and K. Sackinger, *Atmos. Chem. Phys.*, 2012, **12**, 8797–8811.
24 J. T. Middleton, et al., *Plant Dis. Rep.*, 1950, **34**, 245–252.
25 N. L. Bernard, M. J. Gerber, C. M. Astre and M. J. Saintot, *Environ. Sci. Technol.*, 1998, **33**, 217–222.
26 D. Asaf, E. Tas, D. Pedersen, M. Peleg and M. Luria, *Environ. Sci. Technol.*, 2010, **44**, 5901–5907.
27 Y. Tsutsumi, Y. Zaizen and Y. Makino, *Geophys. Res. Lett.*, 1994, **21**, 1727–1730.
28 F. E. Blacet, *Ind. Eng. Chem.*, 1952, **44**, 1339–1342.
29 D. E. Heard and M. J. Pilling, *Chem. Rev.*, 2003, **103**, 5163–5198.
30 K. R. Darnall, A. C. Lloyd, A. M. Winer and J. N. Pitts, *Environ. Sci. Technol.*, 1976, **10**, 692–696.
31 H. Levy, *Science*, 1971, **173**, 141–143.
32 M. R. Kurpius and A. H. Goldstein, *Geophys. Res. Lett.*, 2003, **30**, 1371.
33 S. Li, J. Matthews and A. Sinha, *Science*, 2008, **319**, 1657–1660.
34 K. Salo, M. Hallquist, A. M. Jonsson, H. Saathoff, K. H. Naumann, C. Spindler, R. Tillmann, H. Fuchs, B. Bohn, F. Rubach, T. F. Mentel, L. Muller, M. Reinnig, T. Hoffmann and N. M. Donahue, *Atmos. Chem. Phys.*, 2011, **11**, 11055–11067.
35 J. L. Ambrose, H. Mao, H. R. Mayne, J. Stutz, R. Talbot and B. C. Sive, *J. Geophys. Res.: Atmos.*, 2007, **112**, D21302.
36 R. P. Wayne, I. Barnes, P. Biggs, J. P. Burrows, C. E. Canosamas, J. Hjorth, G. Lebras, G. K. Moortgat, D. Perner, G. Poulet, G. Restelli and H. Sidebottom, *Atmos. Environ., Part A*, 1991, **25**, 1–203.
37 T. Moise, R. K. Talukdar, G. J. Frost, R. W. Fox and Y. Rudich, *J. Geophys. Res.: Atmos.*, 2002, **107**, AAC 6-1.
38 M. Shiraiwa, U. Poschl and D. A. Knopf, *Environ. Sci. Technol.*, 2012, **46**, 6630–6636.
39 Z. Zhao, S. Husainy, C. T. Stoudemayer and G. D. Smith, *Phys. Chem. Chem. Phys.*, 2011, **13**, 17809–17817.
40 A. M. Winer, R. Atkinson and J. N. Pitts, *Science*, 1984, **224**, 156–159.
41 J. H. Seinfeld and S. N. Pandis, *Atmospheric chemistry and physics: from air pollution to climate change*, John Wiley & Sons, 2012.
42 E. Gonzalez-Labrada, R. Schmidt and C. E. DeWolf, *Phys. Chem. Chem. Phys.*, 2007, **9**, 5814–5821.
43 K. Miet, K. Le Menach, P. M. Flaud, H. Budzinski and E. Villenave, *Atmos. Environ.*, 2009, **43**, 3699–3707.
44 R. C. Chapleski, Jr., J. R. Morris and D. Troya, *Phys. Chem. Chem. Phys.*, 2014, **16**, 5977–5986.
45 E. D. Davis, A. Wagner, M. McEntee, M. Kaur, D. Troya and J. R. Morris, *J. Phys. Chem. Lett.*, 2012, **3**, 3193–3198.
46 Y. Liu, J. Liggio, S.-M. Li, D. Breznan, R. Vincent, E. M. Thomson, P. Kumarathasan, D. Das, J. Abbatt, M. Antiñolo and L. Russell, *Environ. Sci. Technol.*, 2015, **49**, 2806–2814.
47 A. J. Tiwari, J. R. Morris, E. P. Vejerano, M. F. Hochella and L. C. Marr, *Environ. Sci. Technol.*, 2014, **48**, 2706–2714.
48 F. A. Houle, W. D. Hinsberg and K. R. Wilson, *Phys. Chem. Chem. Phys.*, 2015, **17**, 4412–4423.
49 Y. Bedjanian and M. L. Nguyen, *Chemosphere*, 2010, **79**, 387–393.
50 E. C. Browne, J. P. Franklin, M. R. Canagaratna, P. Massoli, T. W. Kirchstetter, D. R. Worsnop, K. R. Wilson and J. H. Kroll, *J. Phys. Chem. A*, 2015, **119**, 1154–1163.
51 Y. C. Liu, C. Liu, J. Z. Ma, Q. X. Ma and H. He, *Phys. Chem. Chem. Phys.*, 2010, **12**, 10896–10903.
52 C. Han, Y. C. Liu, J. Z. Ma and H. He, *J. Chem. Phys.*, 2012, **137**, 084507.
53 N. O. A. Kwamena, M. G. Staikova, D. J. Donaldson, I. J. George and J. P. D. Abbatt, *J. Phys. Chem. A*, 2007, **111**, 11050–11058.
54 N. O. A. Kwamena, J. A. Thornton and J. P. D. Abbatt, *J. Phys. Chem. A*, 2004, **108**, 11626–11634.
55 J. Z. Ma, Y. C. Liu and H. He, *Atmos. Environ.*, 2010, **44**, 4446–4453.
56 J. Z. Ma, Y. C. Liu, Q. X. Ma, C. Liu and H. He, *Atmos. Environ.*, 2013, **72**, 165–170.
57 J. J. Nájera, R. Wamsley, D. J. Last, K. E. Leather, C. J. Percival and A. B. Horn, *Int. J. Chem. Kinet.*, 2011, **43**, 694–707.
58 E. Gloaguen, E. R. Mysak, S. R. Leone, M. Ahmed and K. R. Wilson, *Int. J. Mass Spectrom.*, 2006, **258**, 74–85.

59 Y. B. Gai, W. G. Wang, M. F. Ge, H. G. Kjaergaard, S. Jorgensen and L. Du, *Atmos. Environ.*, 2013, **77**, 696–702.
60 S. M. Forrester and D. A. Knopf, *Atmos. Chem. Phys.*, 2013, **13**, 6507–6522.
61 J. Gan, B. Yang, Y. Zhang, X. Shu, C. G. Liu and J. N. A. Shu, *J. Phys. Chem. A*, 2010, **114**, 12231–12236.
62 F. D. Pope, P. J. Gallimore, S. J. Fuller, R. A. Cox and M. Kalberer, *Environ. Sci. Technol.*, 2010, **44**, 6656–6660.
63 J. J. Najera, C. J. Percival and A. B. Horn, *Phys. Chem. Chem. Phys.*, 2009, **11**, 9093–9103.
64 T. L. Eliason, S. Aloisio, D. J. Donaldson, D. J. Cziczo and V. Vaida, *Atmos. Environ.*, 2003, **37**, 2207–2219.
65 P. J. Gallimore, P. Achakulwisut, F. D. Pope, J. F. Davies, D. R. Spring and M. Kalberer, *Atmos. Chem. Phys.*, 2011, **11**, 12181–12195.
66 D. Ray, J. K. Malongwe and P. Klan, *Environ. Sci. Technol.*, 2013, **47**, 6773–6780.
67 J. W. Morris, P. Davidovits, J. T. Jayne, J. L. Jimenez, Q. Shi, C. E. Kolb, D. R. Worsnop, W. S. Barney and G. Cass, *Geophys. Res. Lett.*, 2002, **29**, 71.
68 G. D. Smith, E. Woods, C. L. DeForest, T. Baer and R. E. Miller, *J. Phys. Chem. A*, 2002, **106**, 8085–8095.
69 J. D. Hearn, A. J. Lovett and G. D. Smith, *Phys. Chem. Chem. Phys.*, 2005, **7**, 501–511.
70 B. J. Dennis-Smither, K. L. Hanford, N. O. A. Kwamena, R. E. H. Miles and J. P. Reid, *J. Phys. Chem. A*, 2012, **116**, 6159–6168.
71 E. P. Rosen, E. R. Garland and T. Baer, *J. Phys. Chem. A*, 2008, **112**, 10315–10324.
72 J. E. Ham and J. R. Wells, *Indoor Air*, 2008, **18**, 394–407.
73 T. F. Kahan, N. O. A. Kwamena and D. J. Donaldson, *Atmos. Environ.*, 2006, **40**, 3448–3459.
74 N.-O. A. Kwamena, M. E. Earp, C. J. Young and J. P. D. Abbatt, *J. Phys. Chem. A*, 2006, **110**, 3638–3646.
75 D. Fu, C. B. Leng, J. Kelley, G. Zeng, Y. H. Zhang and Y. Liu, *Environ. Sci. Technol.*, 2013, **47**, 10611–10618.
76 L. Petrick and Y. Dubowski, *Indoor Air*, 2009, **19**, 381–391.
77 C. B. Leng, J. Hiltner, H. Pham, J. Kelley, M. Mach, Y. H. Zhang and Y. Liu, *Phys. Chem. Chem. Phys.*, 2014, **16**, 4350–4360.
78 G. Zeng, S. Holladay, D. Langlois, Y. H. Zhang and Y. Liu, *J. Phys. Chem. A*, 2013, **117**, 1963–1974.
79 S. Raja and K. T. Valsaraj, *J. Air Waste Manage. Assoc.*, 2005, **55**, 1345–1355.
80 Y. Wadia, D. J. Tobias, R. Stafford and B. J. Finlayson-Pitts, *Langmuir*, 2000, **16**, 9321–9330.
81 B. T. Mmereki, D. J. Donaldson, J. B. Gilman, T. L. Eliason and V. Vaida, *Atmos. Environ.*, 2004, **38**, 6091–6103.
82 T. Moise and Y. Rudich, *J. Phys. Chem. A*, 2002, **106**, 6469–6476.
83 T. Moise and Y. Rudich, *J. Geophys. Res.: Atmos.*, 2000, **105**, 14667–14676.
84 S. Enami, M. R. Hoffmann and A. J. Colussi, *J. Phys. Chem. B*, 2008, **112**, 4153–4156.
85 S. Enami, M. R. Hoffmann and A. J. Colussi, *Proc. Natl. Acad. Sci. U. S. A.*, 2008, **105**, 7365–7369.
86 S. Enami, M. R. Hoffmann and A. J. Colussi, *Chem. Res. Toxicol.*, 2009, **22**, 35–40.
87 S. Enami, M. R. Hoffmann and A. J. Colussi, *J. Phys. Chem. A*, 2009, **113**, 7002–7010.
88 S. Enami, M. R. Hoffmann and A. J. Colussi, *J. Phys. Chem. B*, 2009, **113**, 9356–9358.
89 S. Enami, M. R. Hoffmann and A. J. Colussi, *J. Phys. Chem. Lett.*, 2010, **1**, 2374–2379.
90 H. I. Kim, H. Kim, Y. S. Shin, L. W. Beegle, W. A. Goddard, J. R. Heath, I. Kanik and J. L. Beauchamp, *J. Phys. Chem. B*, 2010, **114**, 9496–9503.
91 D. A. Thomas, L. Wang, B. Goh, E. S. Kim and J. L. Beauchamp, *Anal. Chem.*, 2015, **87**, 3336–3344.
92 T. Thornberry and J. P. D. Abbatt, *Phys. Chem. Chem. Phys.*, 2004, **6**, 84–93.
93 H. M. Hung and C. W. Tang, *J. Phys. Chem. A*, 2010, **114**, 13104–13112.
94 B. J. Dennis-Smither, R. E. H. Miles and J. P. Reid, *J. Geophys. Res.: Atmos.*, 2012, **117**, D20204.
95 B. J. Dennis-Smither, F. H. Marshall, R. E. H. Miles, T. C. Preston and J. P. Reid, *J. Phys. Chem. A*, 2014, **118**, 5680–5691.
96 E. Gonzalez-Labrada, R. Schmidt and C. E. DeWolf, *Chem. Commun.*, 2006, 2471–2473.
97 Y. Dubowski, J. Vieceli, D. J. Tobias, A. Gomez, A. Lin, S. A. Nizkorodov, T. M. McIntire and B. J. Finlayson-Pitts, *J. Phys. Chem. A*, 2004, **108**, 10473–10485.
98 J. Vieceli, O. L. Ma and D. J. Tobias, *J. Phys. Chem. A*, 2004, **108**, 5806–5814.
99 T. M. McIntire, A. S. Lea, D. J. Gaspar, N. Jaitly, Y. Dubowski, Q. Q. Li and B. J. Finlayson-Pitts, *Phys. Chem. Chem. Phys.*, 2005, **7**, 3605–3609.
100 J. W. Lu, L. R. Fiegland, E. D. Davis, W. A. Alexander, A. Wagner, R. D. Gandour and J. R. Morris, *J. Phys. Chem. C*, 2011, **115**, 25343–25350.
101 L. R. Fiegland, M. McCorn Saint Fleur and J. R. Morris, *Langmuir*, 2005, **21**, 2660–2661.
102 J. W. Lu and J. R. Morris, *J. Phys. Chem. A*, 2011, **115**, 6194–6201.
103 D. A. Knopf, S. M. Forrester and J. H. Slade, *Phys. Chem. Chem. Phys.*, 2011, **13**, 21050–21062.
104 L. Lee, P. Wooldridge, T. Nah, K. Wilson and R. Cohen, *Phys. Chem. Chem. Phys.*, 2013, **15**, 882–892.
105 S. Gross, R. Iannone, S. Xiao and A. K. Bertram, *Phys. Chem. Chem. Phys.*, 2009, **11**, 7792–7803.
106 D. R. Hanson, A. R. Ravishankara and S. Solomon, *J. Geophys. Res.: Space Phys.*, 1994, **99**, 3615–3629.
107 M. Shiraiwa, C. Pfrang and U. Poeschl, *Atmos. Chem. Phys.*, 2010, **10**, 3673–3691.
108 M. Shiraiwa, R. M. Garland and U. Poschl, *Atmos. Chem. Phys.*, 2009, **9**, 9571–9586.
109 M. Schutze and H. Herrmann, *J. Atmos. Chem.*, 2005, **52**, 1–18.
110 Y. Zhang, B. Yang, J. Gan, C. G. Liu, X. Shu and J. N. Shu, *Atmos. Environ.*, 2011, **45**, 2515–2521.
111 Y. F. Wang, P. Zhang, B. Yang, C. G. Liu and J. N. Shu, *Chemosphere*, 2013, **90**, 848–855.

112 C. G. Liu, B. Yang, J. Gan, Y. Zhang, M. Liang, X. Shu and J. N. Shu, *Chemosphere*, 2012, **87**, 470–476.
113 D. A. Knopf, J. Mak, S. Gross and A. K. Bertram, *Geophys. Res. Lett.*, 2006, **33**, L17816.
114 S. Gross and A. K. Bertram, *J. Geophys. Res.: Atmos.*, 2009, **114**, D02307.
115 Y. Zhang, R. C. Chapleski, J. W. Lu, T. H. Rockhold, D. Troya and J. R. Morris, *Phys. Chem. Chem. Phys.*, 2014, **16**, 16659–16670.
116 J. D. Smith, J. H. Kroll, C. D. Cappa, D. L. Che, C. L. Liu, M. Ahmed, S. R. Leone, D. R. Worsnop and K. R. Wilson, *Atmos. Chem. Phys.*, 2009, **9**, 3209–3222.
117 I. J. George, A. Vlasenko, J. G. Slowik, K. Broekhuizen and J. P. D. Abbatt, *Atmos. Chem. Phys.*, 2007, **7**, 4187–4201.
118 B. D'Anna, O. Andresen, Z. Gefen and C. J. Nielsen, *Phys. Chem. Chem. Phys.*, 2001, **3**, 3057–3063.
119 S. Mitroka, S. Zimmeck, D. Troya and J. M. Tanko, *J. Am. Chem. Soc.*, 2010, **132**, 2907–2913.
120 J. X. Zhang, L. Yang and D. Troya, *Chin. J. Chem. Phys.*, 2013, **26**, 765–773.
121 C. R. Ruehl, T. Nah, G. Isaacman, D. R. Worton, A. W. H. Chan, K. R. Kolesar, C. D. Cappa, A. H. Goldstein and K. R. Wilson, *J. Phys. Chem. A*, 2013, **117**, 3990–4000.
122 K. R. Kolesar, G. Buffaloe, K. R. Wilson and C. D. Cappa, *Environ. Sci. Technol.*, 2014, **48**, 3196–3202.
123 A. Vlasenko, I. J. George and J. P. D. Abbatt, *J. Phys. Chem. A*, 2008, **112**, 1552–1560.
124 I. J. George, R. Y. W. Chang, V. Danov, A. Vlasenko and J. P. D. Abbatt, *Atmos. Environ.*, 2009, **43**, 5038–5045.
125 T. Nah, S. H. Kessler, K. E. Daumit, J. H. Kroll, S. R. Leone and K. R. Wilson, *Phys. Chem. Chem. Phys.*, 2013, **15**, 18649–18663.
126 J. H. Slade and D. A. Knopf, *Phys. Chem. Chem. Phys.*, 2013, **15**, 5898–5915.
127 C. Lai, Y. Liu, J. Ma, Q. Ma and H. He, *Phys. Chem. Chem. Phys.*, 2015, **17**, 10953–10962.
128 C. Lai, Y. Liu, J. Ma, Q. Ma and H. He, *Atmos. Environ.*, 2014, **91**, 32–39.
129 M. Pflieger, A. Monod and H. Wortham, *Environ. Sci. Technol.*, 2013, **47**, 6239–6246.
130 M. Al Rashidi, A. Chakir and E. Roth, *Atmos. Environ.*, 2014, **82**, 164–171.
131 M. Segal-Rosenheimer, R. Linker and Y. Dubowski, *Phys. Chem. Chem. Phys.*, 2011, **13**, 506–517.
132 Y. C. Liu, J. Liggio, T. Harner, L. Jantunen, M. Shoeib and S. M. Li, *Environ. Sci. Technol.*, 2014, **48**, 1041–1048.
133 Y. Liu, L. Huang, S. M. Li, T. Harner and J. Liggio, *Atmos. Chem. Phys.*, 2014, **14**, 12195–12207.
134 Y. Liu, S. M. Li and J. Liggio, *Atmos. Chem. Phys.*, 2014, **14**, 9201–9211.
135 V. F. McNeill, R. L. N. Yatavelli, J. A. Thornton, C. B. Stipe and O. Landgrebe, *Atmos. Chem. Phys.*, 2008, **8**, 5465–5476.
136 T. M. D'Andrea, X. Zhang, E. B. Jochnowitz, T. G. Lindeman, C. Simpson, D. E. David, T. J. Curtiss, J. R. Morris and G. B. Ellison, *J. Phys. Chem. B*, 2008, **112**, 535–544.
137 T. Nah, S. H. Kessler, K. E. Daumit, J. H. Kroll, S. R. Leone and K. R. Wilson, *J. Phys. Chem. A*, 2014, **118**, 4106–4119.
138 T. Nah, H. Zhang, D. R. Worton, C. R. Ruehl, B. B. Kirk, A. H. Goldstein, S. R. Leone and K. R. Wilson, *J. Phys. Chem. A*, 2014, **118**, 11555–11571.
139 A. K. Bertram, A. V. Ivanov, M. Hunter, L. T. Molina and M. J. Molina, *J. Phys. Chem. A*, 2001, **105**, 9415–9421.
140 C. Iuga, R. E. Olea and A. Vivier-Bunge, *J. Mex. Chem. Soc.*, 2008, **52**, 36–46.
141 C. Iuga, A. Vivier-Bunge, A. Hernandez-Laguna and C. I. Sainz-Diaz, *J. Phys. Chem. C*, 2008, **112**, 4590–4600.
142 C. W. Dilbeck and B. J. Finlayson-Pitts, *Phys. Chem. Chem. Phys.*, 2013, **15**, 9833–9844.
143 S. G. Moussa and B. J. Finlayson-Pitts, *Phys. Chem. Chem. Phys.*, 2010, **12**, 9419–9428.
144 E. R. Mysak, J. D. Smith, P. D. Ashby, J. T. Newberg, K. R. Wilson and H. Bluhm, *Phys. Chem. Chem. Phys.*, 2011, **13**, 7554–7564.
145 K. L. King, G. Paterson, G. E. Rossi, M. Iljina, R. E. Westacott, M. L. Costen and K. G. McKendrick, *Phys. Chem. Chem. Phys.*, 2013, **15**, 12852–12863.
146 D. Troya, *Theor. Chem. Acc.*, 2012, **131**, 1072.
147 C. Waring, K. L. King, P. A. J. Bagot, M. L. Costen and K. G. McKendrick, *Phys. Chem. Chem. Phys.*, 2011, **13**, 8457–8469.
148 P. A. J. Bagot, C. Waring, M. L. Costen and K. G. McKendrick, *J. Phys. Chem. C*, 2008, **112**, 10868–10877.
149 M. Roeselová, J. Vieceli, L. X. Dang, B. C. Garrett and D. J. Tobias, *J. Am. Chem. Soc.*, 2004, **126**, 16308–16309.
150 S. Enami, M. R. Hoffmann and A. J. Colussi, *J. Phys. Chem. Lett.*, 2015, **6**, 527–534.
151 S. Enami, M. R. Hoffmann and A. J. Colussi, *J. Phys. Chem. A*, 2014, **118**, 4130–4137.
152 L. E. Hatch, J. M. Creamean, A. P. Ault, J. D. Surratt, M. N. Chan, J. H. Seinfeld, E. S. Edgerton, Y. X. Su and K. A. Prather, *Environ. Sci. Technol.*, 2011, **45**, 5105–5111.
153 P. Q. Fu, K. Kawamura, Y. F. Cheng, S. Hatakeyama, A. Takami, H. Li and W. Wang, *Atmos. Chem. Phys.*, 2014, **14**, 4185–4199.

